Optimization Study Relevant to Louvered Fin Compact Heat Exchangers

R. A. Stephan and K. A. Thole
Virginia Tech
Mechanical Engineering Department
Blacksburg, VA 24061

Corresponding Author: K. A. Thole, thole@vt.edu
(540)231-7192 and FAX (540)231-9100

Submitted for Review: *International Journal of Heat Exchangers*
July 2003

Abstract

Louvered fins provide a method for improving the heat transfer performance of compact heat exchangers by initiating the growth of new boundary layers. The growth leads to average convective heat transfer coefficients being higher than that which would occur for a continuous fin. It is desirable to optimize the louver fin to provide reduced fan power and increased heat transfer. This paper presents a numerical method for optimizing a compact heat exchanger design. The results of the current study show that optimization methods used in conjunction with CFD can be used to improve the performance of a louvered fin compact heat exchanger. Of the physically realizable geometries considered, better performance for a compact heat exchanger can be achieved for small fin pitches and small louver angles.

1. Introduction

Compact heat exchangers are typically used as radiators to remove the excess thermal energy in many automotive applications and, as such, the efficiency is quite important for this financially competitive industry. Radiators, similar to that shown in figure 1, are used extensively in this industry because of their minimal space requirements and high heat removal

capabilities. Louvered fins within the heat exchanger, rather than continuous fins, are commonly used to break up the boundary layer formation thereby providing high average heat transfer coefficients along the air side relative to that occurring on continuous fins.

A typical compact heat exchanger uses two fluids (air and liquid coolant) to exchange energy by conduction through and convection along louvered fin surfaces. In this configuration, the total thermal resistance associated with the system can be divided into three parts. First there is the thermal resistance that occurs due to the convection on the coolant side of the heat exchanger, which makes up approximately 15% of the total thermal resistance. Second there is the conduction through the tube wall that accounts for less than 1% of the overall thermal resistance. The thermal resistance on the air side of the louvered fin compact heat exchanger is the third component and is responsible for approximately 85% of the total thermal resistance. It is apparent from the distribution of thermal resistances that the performance of a louvered fin heat exchanger can be improved by focusing optimization efforts on the air side. The optimization method shown in this paper focuses on optimizing the air side heat exchange for a louvered fin compact heat exchanger from the following considerations: increasing the heat transfer, reducing the fan power, and minimizing the volume required.

Several objectives were defined for this research effort. The first objective set forth was to benchmark the computational fluid dynamics (CFD) predictions to ensure accurate computations. This objective was completed by comparing the CFD predictions to experimentally obtained heat transfer coefficients along the louver of the fin. The second objective was to demonstrate how a combined CFD and optimization package could be used to improve the performance of a louvered fin compact heat exchanger. The third goal was to evaluate a range of fin pitches and louver angles for feasible compact heat exchanger designs to determine an optimal design.

2. Literature Review

While there is a plethora of relevant compact heat exchanger studies presented in the literature, only a few studies will be discussed for the purpose of this paper. The most relevant of these studies to the current work was performed by Suga and Aoki (1991). They completed a numerical study using a two-dimensional finite difference code to determine the optimum combination of geometrical parameters for a louvered fin array. Suga and Aoki's study focused

on the slower flow regime corresponding to Reynolds numbers between 64 and 450. They also limited their study to a fin pitch to louver pitch ratio of $F_p/L_p < 1.125$ and $20° < \theta < 30°$. In these numerical simulations, the louver angle, fin pitch, and fin thickness were varied to determine the optimum combination of fin parameters. To find the optimal geometry, Suga and Aoki correlated the released heat per unit volume to the amount of pumping power required. From the combined perspective of heat transfer and pressure drop, smaller louver angles were found to perform better and as such, the optimal geometry was determined to be a $F_p/L_p = 0.50$, $\theta = 20°$ model.

Chang and Wang (1997) performed two relevant studies to the present work. In the first study, they proposed a correlation for the average Colburn factors in a louvered fin array. The resultant pressure drop for the same louver geometries was presented in the second study (2000). To develop correlations for the heat transfer and pressure drop, Chang and Wang collected the experimental data for 91 different louver geometries from several earlier studies with a combined total of 1109 data points. Their correlation was valid for $100 < Re_{Lp} < 3000$ and predicted 89% of the louvered fin data within 15% with a mean deviation of 7.6%. The Colburn factor correlation showed that the heat transfer coefficient tends to increase with decreasing fin pitch and increasing louver angle. As mentioned above, Chang and Wang also developed a correlation for the friction factor in a louvered fin array. The friction factor correlation was valid for $150 < Re_{Lp} < 5000$ and predicted 83% of the data within 15% with a mean deviation of 9.2%. Chang and Wang's correlation agreed with the results of Suga and Aoki in showing that the pressure drop tended to decrease with large values of fin pitch and small values of louver angle.

It is apparent from these earlier studies that the louver angle and fin pitch trends tend to work against each other when discussing the optimization of a heat exchanger from a combined perspective of heat transfer and pressure drop. For this reason, it is necessary to look at the effect of louver angle and fin pitch on the overall performance of a louvered fin heat exchanger The work presented in the current paper encompasses a much larger range of fin pitches as will be discussed in the following sections.

3. Computational and Optimization Methodologies

The two-dimensional Navier-Stokes and energy equations were solved using the commercially available Fluent 5.0. The CFD predictions were obtained by solving the mass,

momentum, and energy equations using second order discretization. The flow was assumed tc be laminar and steady. The computational models consisted of a single fin row with 17 streamwise louvers including one entrance louver, one exit louver, and one flow reversal (turning) louver. The model was built and meshed in the pre-processor program Gambit, which is a mesh generation program packaged with Fluent. To computationally simulate an infinite stack of louvers, periodic boundary conditions were applied to the top and bottom of the flow domain. A constant inlet velocity, corresponding to $Re_{Lp} = 1016$, was applied at three louver pitches upstream of the entrance louver while an outflow boundary condition was applied at 6.5 louver pitches downstream of the exit louver. A constant heat flux was assigned to the front and back side of each louver in the array. A schematic showing all of the boundary conditions is shown in figure 2.

The mesh used for the model consisted of a triangular grid for the majority of the louver passage with a quadrilateral grid placed along the surface boundaries of the louver. Figure 3 shows the "boundary layer" mesh used around the louvers as well as the triangular mesh used throughout the majority of the flowfield. The detailed quadrilateral mesh around the louver consisted of ten rows of cells that spanned a total distance of approximately half of the louver thickness on each side of the louver. Grid sensitivities were assessed using mesh sizes ranging from 150,000 to 500,000 cells. The predictions indicated that a mesh size consisting of 500,000 cells, which was used for the computations presented in this paper, was grid insensitive.

To expedite the solving process, 800 iterations were executed solving the momentum equations then the energy equation was turned on and allowed to converge. The entire process took approximately 1100 iterations to ensure acceptable convergence. Acceptable convergence occurred when the momentum and energy residuals dropped by three and four orders of magnitude, respectively, between iterations. The computations were executed on an SGI Origin 2000 using four parallel processors and required approximately 2 hours for each case to be completed.

The optimization of the louver geometry was completed by integrating the optimization software, iSIGHT, with the Gambit and Fluent journal files (Lethander et al., 2003). Journal files created by Gambit are text files that contain the program commands to be executed. The journal files are read by the Gambit executable and describe how the geometry should be created and

meshed. For each computation that was performed, the Gambit journal file contained variables that were modified for a particular geometry.

The optimization process began with iSIGHT entering the input parameters that described the louver geometry into the Gambit journal files. After the geometry was created and meshed in Gambit, Fluent was used to solve the two-dimensional Navier-Stokes and energy equations. The optimization variables were then obtained from the Fluent output files and the geometric parameters were changed according to the optimization technique being employed by iSIGHT. This change was based on the objective function defined for the study. For the optimization study being presented in this paper, an exploratory optimization technique called simulated annealing was used. Because this technique avoids focusing only on a local region of the design space, simulated annealing provides good coverage of the entire design space in its search for an optimal design.

As mentioned above, several values were held constant throughout the optimization. The entire study was performed for a single Reynolds number of $Re_{Lp} = 1016$. Both the louver pitch and the fin thickness also remained constant for the simulations. The louver surfaces were considered to have a constant heat flux and the optimization variables considered for this particular study were the fin pitch and the louver angle. The design constraints included the following: $0.58 < F_p/L_p < 2.00$ and $15° < \theta < 45°$. To insure a feasible design space that could be physically realized, it was necessary to perform the optimization in 10° increments. Table 1 shows the louver angle ranges along with the allowable values of F_p/L_p.

In performing the optimization for the louvered fin heat exchanger geometry an objective function needed to be defined. One of the performance characteristics considered was the heat dissipated by the louver array (Q), which is given as

$$Q = q'' \cdot A_{louvers} = C_1 \qquad (1)$$

where q'' represents the heat flux applied to the surface of each louver and A represents the sum of all the louver surface areas exposed to the flow. While in reality a fin experiences neither a fully constant heat flux nor a constant surface temperature, we chose a constant heat flux boundary condition. The total surface area exposed to the flow as well as the surface heat flux remained the same between the different louver geometries therefore, equation 1 was equal to a constant.

A second characteristic of the heat exchanger considered was the volume of the core (V). Minimizing the volume of the core is done to reduce the amount of space that a heat exchanger occupies as well as reduce the overall weight of the system. The volume of the core is defined by the following relationship

$$V = F_p \cdot w \cdot L = C_2 \cdot F_p \tag{2}$$

In equation 2, w is the width of the heat exchanger core and L represents the streamwise length of the entire louver array. Both L and w were held constant for the purposes of this study.

Lastly, another characteristic of a heat exchanger considered is the pumping power required to push the flow through the louver array. The pumping power required (P) is given as

$$P = U_{in} * F_p * w * \Delta p = C_3 * F_p * \Delta p \tag{3}$$

Where U_{in} is the inlet velocity to the louver array and Δp represents the pressure drop through the entire louver array. As before, several of the terms in equation 3 are constant between the different louver geometries.

From these considerations, an objective function was defined as follows

$$\frac{Q}{V * P} = \frac{C_1}{C_2 F_p C_3 F_p \Delta p} \propto \frac{1}{F_p^2 \Delta p} \tag{4}$$

To accomplish the goals of the optimization, maximizing the function given in equation 4 was considered as the objective function. Prior to any computations being performed, a benchmarking of the predictions with experimental data was performed.

4. Experimental Methodology

The CFD predictions were benchmarked using experimental results from a study performed in conjunction with the current optimization study. A complete documentation of those results are given in Lyman et al. (2002). The experimental design was made to insure that meaningful, spatially-resolved heat transfer coefficients could be made along several streamwise

louver positions over a wide range of Reynolds numbers. To insure good measurement resolution, the experimental louver models were scaled up by a factor of 20.

A schematic of the open-loop test rig used for this study is shown in figure 4. The inlet of the test assembly consisted of honeycomb, a screen, and a contraction that together provided a uniform flowfield at the entrance to the test section. The nozzle geometry was designed using the aforementioned CFD package, Fluent, and had a 16:1 area reduction from the front of the nozzle to the entrance of the test section. The velocity distribution at the inlet of the test section was shown to be uniform using Laser Doppler velocimeter measurements. A variable speed centrifugal fan located at the exit of the test rig provided the flow through the set-up with the speed of the fan being controlled using an AC inverter. The flow rate was measured using a laminar flow element located immediately downstream of the test section.

The louver test section containing the louver array was a two-dimensional idealization of an actual heat exchanger. Each of the louver geometries tested had 17 louvers in the streamwise direction, while the number of fin rows (louver passages) varied between the different models. The model with the smallest fin pitch had 11 rows while the largest fin pitch had only 9. For all cases, periodicity was verified between rows. Louver heat transfer measurements were made along louvers 2-8 while a constant heat flux boundary condition was applied along louver 1-8. In each of the models, the louver pitch and fin thickness were held constant ($t/L_p = 0.082$) while the fin pitch and louver angle were varied. Springer and Thole (1998) observed the flowfield to be louver directed, so styrofoam plates that matched the louver angle were used on the interior of the test section to create a periodic flow. The periodic flow condition more accurately simulated an infinite stack of louver rows. The Styrofoam plates reduced endwall effects associated with the top and bottom of the test section as well as minimize any conduction losses through the top and bottom of the test section.

A constant heat flux boundary condition was applied to all of the louvers upstream of the turning louver by using thin heating foils as shown in figure 5. The core of the louvers was balsa wood, which minimized the conduction through the louvers. This core was sandwiched between file folder paper, which further insulated the louver and provided the correct louver thickness. The outside layers of the louver consisted of a stainless steel foil that served as the resistive heating element. Lead wires were connected using copper bus bars that were soldered to both ends of the stainless steel foils.

The heat flux values were chosen so that the temperature distribution across the louver surface in the streamwise direction would be the same for each of the Reynolds numbers. The resistive heating elements were connected in series to ensure a constant current through each louver. Because the surface area of the entrance louvers was 1.9 times larger than that of the downstream louvers, two separate circuits were needed. The electrical resistance of the louvers were measured to be 0.15±2% Ω for the main field louvers and 0.078±2% Ω for the entrance louvers. The current through the circuits was determined by measuring the voltage drop across precision resistors located in the circuits. The surface heat flux was then calculated using the heater resistance and the current through the circuit.

The surface temperatures of the louvers were measured using thermocouples embedded in the balsa wood core, as shown in figure 6, for two instrumented louvers. The thermal resistance of the foil was relatively small when compared to the convective resistance ($R_{foil}/R_{convection} = 2 \times 10^{-5}$ in most cases) and was therefore neglected. Two-dimensionality was also verified through the use of louvers instrumented with a number of spanwise thermocouples. 27 were installed along the streamwise distance of the louver on both the front and back sides at the spanwise center of the louver. Due to the complexity of the velocity and thermal fields that develop as the air flows through the louver array, the temperature distributions on the front and back sides of the louvers were not identical. Prior to calculating the heat transfer coefficients, a conduction correction was made due to the temperature difference between the windward and leeward surfaces.

The uncertainties of experimental quantities were computed by using the method presented by Moffat (1988). The uncertainty was calculated by acquiring the derivatives of the desired variable with respect to individual experimental quantities and applying known uncertainties. The combined precision and bias uncertainty of the individual temperature measurements was ± 0.15 °C, which dominated the other uncertainties. The uncertainties in the Nusselt number were the highest for the $Re_{Lp} = 230$ condition at the leading edge of the second louver where the temperature differences between the surface and fluid were small. At this location, the uncertainties ranged as high as 11.4%. Uncertainties decreased along the louver where more representative numbers were 6.0%. For the $Re_{Lp} = 1016$ flow condition, the uncertainties in the Nusselt numbers were 4.2% along most of the louvers.

5. Verification of CFD Predictions

In an effort to validate the use of a CFD code for the optimization study, it was imperative to show that the code could accurately predict the heat transfer measurements in the experimental apparatus mentioned earlier. The verification was performed by comparing the CFD predicted Nusselt numbers to those obtained during the experiments. Note that the heat transfer coefficients in the Nusselt number were defined based on the bulk temperature at the inlet to the particular louver passage. This results in Nusselt numbers that are sensitive to the local fluid temperature, which is a function of the thermal wake from the upstream louvers.

Figure 7 shows a comparison between the experimentally measured heat transfer coefficients and the CFD predictions for a $F_p/L_p = 0.91$ and louver angle of $\theta = 20°$ at the seventh louver position. The comparison is shown for a $Re_{Lp} = 1016$. There is relatively good agreement between the measurements and CFD predictions. Although this comparison is only shown for one geometry at one louver position, it is representative of the comparisons made to date. Comparisons have been made for three different louver pitches at two different Reynolds numbers, all showing good agreement between the experiments and computations for a majority of the louver surfaces. For the second and third louver positions, however, the agreement between the measurements and predictions was not as good because of the flow separation predicted at the leading edge of the louver, which was predicted to be more severe than the measurements indicated. This is mostly attributed to the fact that sharp leading edges were modeled whereby the edges were more rounded in the experiments. Apart from the leading edge regions of the second and third louver positions, however, the CFD predictions were typically well within the experimental uncertainty bands shown by the broken lines in figure 7.

6. Thermal Wake Progression

Lyman et al. (2002) showed that the thermal field surrounding a particular louver is the overriding influence on the heat transfer for that louver. For example, if the fluid surrounding a particular louver is hot, the heat transfer from that louver will be relatively low. Hot local fluid temperatures are typically caused by an upstream thermal wake impinging onto the louver surface. As discussed previously, each of the louver surfaces had a constant surface heat flux and, as such, the entrance louver transferred approximately two times the amount of energy to the flow as compared with the downstream louvers because of the larger surface area of the

entrance louvers relative to the downstream louvers. Consequently, the flow leaving the entrance louvers created a significantly hotter thermal wake than the wakes exiting the downstream louvers. For this reason, it is important to track the progression of the entrance louver's thermal wake when evaluating the performance of a louver array.

Figures 8-12 show the louver arrays for two of the louver geometries studied as well as information about the thermal wake's progression through the louver array for $Re_{Lp} = 230$ and $Re_{Lp} = 1016$. The solid black lines extending from the trailing edge of the entrance louver show how a thermal wake would progress if it were completely louver-aligned. All surfaces having a measured louver-averaged temperatures that were greater than the local bulk temperature entering the passages are shown as filled louver surfaces. These measurements were reported in detail by Lyman, et al. (2002), but are summarized in this paper in figures 8-12. In studying figures 8-12, several general trends are obvious and will be discussed in the following paragraphs.

The first trend indicated is that the thermal wakes from the entrance louver are hotter and maintain form further downstream at higher Reynolds numbers. The first occurrence of this is shown in figures 8 and 9 for the $F_p/L_p = 0.91$, $\theta = 20°$ model. For the higher Reynolds number of $Re_{Lp} = 1016$, the thermal wake from the entrance louver impacts both fourth and seventh louvers, as shown in figure 9. In contrast at $Re_{Lp} = 230$, as shown in figure 8, none of the louvers are impacted by the thermal wake. Another example of this progression is shown for a $F_p/L_p = 0.91$, $\theta = 27°$ model in figures 10-11. In this model, the third louver is impacted by the thermal wake for both Reynolds numbers. However, for the higher Reynolds number case of $Re_{Lp} = 1016$ shown in figure 11, the thermal wake proceeds to impact both the fifth and seventh louvers, which does not occur for the $Re_{Lp} = 230$ case. Both of these examples show that the thermal wakes from the entrance louver maintain form further downstream at higher Reynolds numbers which agrees with observations made by Springer and Thole (1999).

The second trend is that a more duct-directed flow in the louvered fin array re-directs the thermal wake in the axial direction. This typically occurs for the models having a large F_p/L_p ratio because the flow entering the array tends to remain duct-directed. This effect is also more pronounced at $Re_{Lp} = 1016$ than 230 because the flow entering the array has more momentum in the streamwise direction. Figure 9 illustrates this wake progression for the $F_p/L_p = 0.91$, $\theta = 20°$ model at $Re_{Lp} = 1016$. The black line extending from the entrance louver shows that the

entrance louver is geometrically aligned with the sixth louver; however, the thermal wake impacts the fourth and seventh louvers as shown by the solid louvers. To further illustrate the effect of the large F_p/L_p ratio, we considered a much larger fin pitch model. Figure 12, which shows a fin pitch of $F_p/L_p = 1.22$ and $\theta = 39°$ model at $Re_{Lp} = 1016$, indicates that louvers 4 and 7 are geometrically aligned with the entrance louver. The thermal wake from the entrance louver, however, follows a more duct-directed path causing the thermal wake to impact the front and back surfaces of the third louver.

As shown by these examples, it is imperative to understand the progression of the entrance louver's thermal wake when designing and evaluating the performance of a louver array for use in a louvered fin compact heat exchanger. The previous section indicates that one must model the entire louver array either computationally or experimentally in order to show how the downstream louvers are impacted by the thermal wakes from upstream louver, particularly the entrance louver. Unfortunately, one cannot just look at the geometry of a louver array *a priori* and determine the progression of the entrance louver's thermal wake. For this reason, the current optimization study was performed.

7. Optimization Results

The optimization study that was performed consisted of approximately 120 different simulated cases. As mentioned above, the goal of the optimization study was to maximize the right hand side of the relationship defined in equation 4. Figure 13 shows the optimization results with the optimization function separated into the two terms in equation 4. The first part, which is shown on the right axis, is $1/F_p^2$ while the second part is simply $1/\Delta p$. The reason for evaluating the optimization function as two separate parts is to show the contribution of each on the overall value for the optimization function. The $1/F_p^2$ has values that range between 250 and 4000, while the $1/\Delta p$ maintains values between 0.5 and 2.5. From the above discussion and figure 13, it is apparent that the $1/F_p^2$ value dominates the optimization function in terms of order of magnitude and is clearly a predictable trend. These results indicate a small F_p/L_p is desirable for a compact heat exchanger design. The pressure drop term, however, is the term that compares the relative performance of the heat exchanger designs at each F_p/L_p.

Figure 14 shows the optimization function plotted as a function of louver angle (θ) for small bands of F_p/L_p. The predictions presented in figure 14 indicate that as the louver angle is

increased, the value of the optimization function decreases, which is a result of the flow becoming more axially-directed, as discussed in the previous section. Also, there is a much wider spread of the optimization function at the lower louver angles indicating a relatively strong F_p/L_p dependence than at the higher louver angles where the predictions fall into a more narrow band. For several fin pitch bands, the values of the optimization function maintain a relatively constant value as the louver angle is increased for the louver angle range of $15° < \theta < 30°$. However, as θ is increased beyond 30° the optimization function significantly decreases. The reason for this sudden decrease at these high louver angles is that there exists a tendency for flow separation. These effects cause the pressure drop through the louver array to increase as the louver angle is increased.

Figures 15 through 17 show the optimization function plotted as a function of F_p/L_p for three louver angle bands that were studied. Figure 15 shows the optimization function for $15°<\theta<25°$, which was the smallest louver angle range that was studied. It is apparent that the optimization function decreases at a relatively constant slope for the majority of the predictions. While this is true, there are several data points that do not fall within the linear trend of the data. The outliers on the plot correspond to the louver angles of $\theta > 21°$. The reason for these outliers, as alluded to earlier in this section, is the impact of the flow separation on the pressure drop.

The data for $25° < \theta < 35°$, shown in figure 16, indicates no easily identifiable trends. For the lower louver angles, the optimization function does decrease with increasing values of F_p/L_p showing the dominance of the fin pitch term. However, at the higher louver angles, such as $33° < \theta < 34°$, the predictions actually increase with increasing values of F_p/L_p ($1/F_p^2\Delta p = 650$ to 800 for $F_p/L_p = 1.5$ to 1.6). Even more scatter is indicated in figure 18 whereby the optimization function actually increases with increasing F_p/L_p for $40° < \theta < 42°$ due to the increased pressure drop associated with the larger louver angles. Note the relatively poor performance of these high louver angled designs relative to that of the lower louver angles.

These results agree quite well with those presented by Suga and Aoki (1991). As mentioned above, they estimated the performance of louvered fin heat exchangers by discussing the correlation between the amount of heat released by a heat exchanger and the pumping power required to operate it. In doing so, they evaluated the ratio of the total heat released and the volume of the fin core as well as the ratio of the pumping power to the volume of the core. Suga

and Aoki concluded that models with smaller fin pitches and louver angles performed best from a combined viewpoint of both heat transfer and pressure drop, and as such, they stated that the $F_p/L_p = 0.50$, $\theta = 20°$ model was the optimal model. Of course, $F_p/L_p = 0.50$ was the smallest fin pitch they studied as was $\theta = 20°$ the smallest louver angle studied.

Chang and Wang (1997) presented generalized correlations for both heat transfer and pressure drop performances of louvered fin heat exchangers. In studying the ratio of Colburn factor (dimensionless heat transfer coefficient) to friction factor, it was apparent that the optimal louver geometry would be one with a large fin pitch and low louver angle. The observation that the optimal geometry would have a small louver angle agrees with the results presented by Suga and Aoki as well as those shown in this paper. However, the current results are in disagreement regarding the large fin pitch. This difference can be explained by focusing on the comparison of the "optimization functions" used for each of the studies. The current study as well as the study completed by Suga and Aoki focused on reducing the volume of the core as well as minimizing the pressure drop while maximizing the heat released. In order to minimize the volume of the core, it is necessary to reduce the fin pitch of the louvered fin model as shown in equation 2. In the evaluation of Chang and Wang's trends, the volume of the core was not accounted for the in the ratio of Colburn factor to friction factor.

8. Conclusions

The results of this study indicate the importance of understanding the flow field of a louvered fin compact heat exchanger. The progression of the thermal wakes is not easily discernable for this complicated flow field and, as such, it is not easy to design an efficient compact heat exchanger through geometrical considerations alone. The results of this study do indicate the validity and value of using computational fluid dynamics to simulate the flow through a compact heat exchanger. Benchmarking with highly-resolved heat transfer measurements along a louver surface indicated relatively good agreement between the predictions and measurements.

Once a good benchmark was achieved, the results in this paper indicated the benefit of using an optimization methodology as a viable technique for designing compact heat exchangers. Using the approach of a simulated annealing optimization method, an engineer can save a large amount of time in the design phase of a louvered fin array by exploring a large solution domain

For the optimization function used throughout this study, the optimal design was found to be a very strong function of the fin pitch for the given problem constraints. That being said, the optimization function became dependent on the louver angle. According to the derived optimization objective, the best performing heat exchanger geometry from a combined heat transfer and pressure drop point of view is one having a small ratio of fin pitch to louver pitch at small louver angles.

9. References

Chang, Y. and Wang, C. (1997) "A Generalized Heat Transfer Correlation for Louver Fin Geometry," *International Journal of Heat and Mass Transfer*, Vol. 40, No. 3, pp. 533-544.

Chang, Y., Hsu, K., Lin, Y., Wang, C. (2000) "A Generalized Friction Correlation for Louver Fin Geometry," International Journal of Heat and Mass Transfer, Vol. 43, No. 12, pp.2237-2243.

iSIGHT Designer's Guide, 1999, Version 5.0, Engineous Software, Inc., North Carolina.

Fluent User's Guide (1998) Release 5.0, Fluent, Inc., New Hampshire.

Lethander, A.,Thole, K. A., Zess, G., and Wagner, J., 2003, "Optimizing the Vane-Endwall Junction to Reduce Adiabatic Wall Temperatures in a Turbine Vane Passage" ASME GT2003-38940.

Lyman, A. C., Stephan, R. A., and Thole, K. A., Zhang, L., Memory, S., 2002 "Scaling of Heat Transfer Coefficients Along Louvered Fins," *Experimental Thermal Fluid Science*, vol. 26, no. 5, pp 547-563.

Moffat, R. J., 1988, "Describing the Uncertainties in Experimental Results," *Experimental Thermal and Fluid Science*, 1, 3-17.

Springer, M.E., and Thole, K. A., 1998, "Experimental Design for Flowfield Studies of Louvered Fins," *Experimental Thermal and Fluid Science*, vol. 18, no. 3, pp. 258-269.

Springer, M. E. and Thole, K. A., 1999, "Entry Region of Louvered Fin Heat Exchangers," *Experimental Thermal and Fluid Science*, Vol. 19, pp. 223-232.

Suga, K. and Aoki, H. (1991) "Numerical Study on Heat Transfer and Pressure Drop in Multilouvered Fins," *ASME/JSME Thermal Engineering Proceedings*, Vol. 4., pp. 361-368.

Table 1. Fin Pitch And Louver Angle Ranges For Optimization Study

θ (degrees)	F_p/L_p
15° < θ < 25°	0.58 < F_p/L_p < 2.0
25° < θ < 35°	0.73 < F_p/L_p < 2.0
35° < θ < 45°	0.88 < F_p/L_p < 2.0

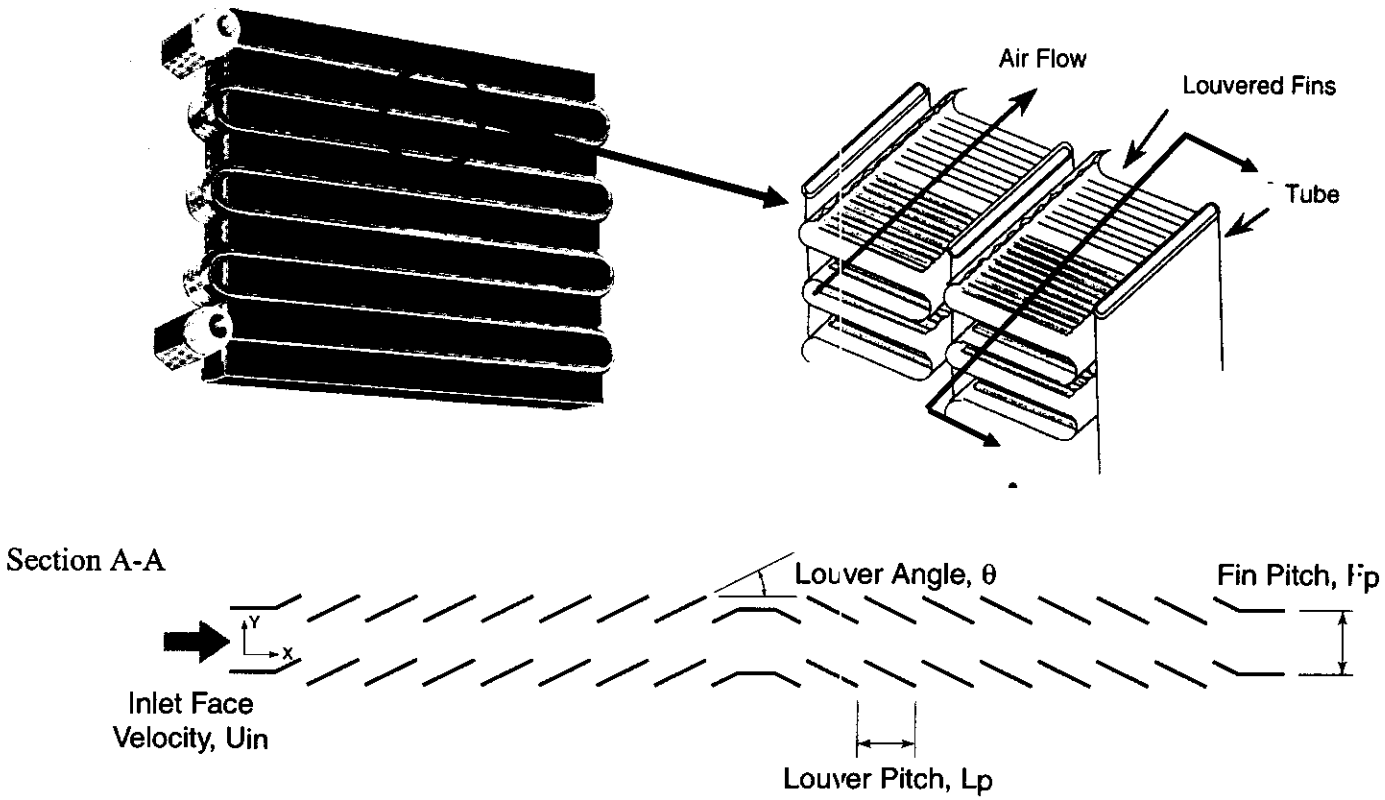

Figure 1 Typical geometry for a louvered fin heat exchanger.

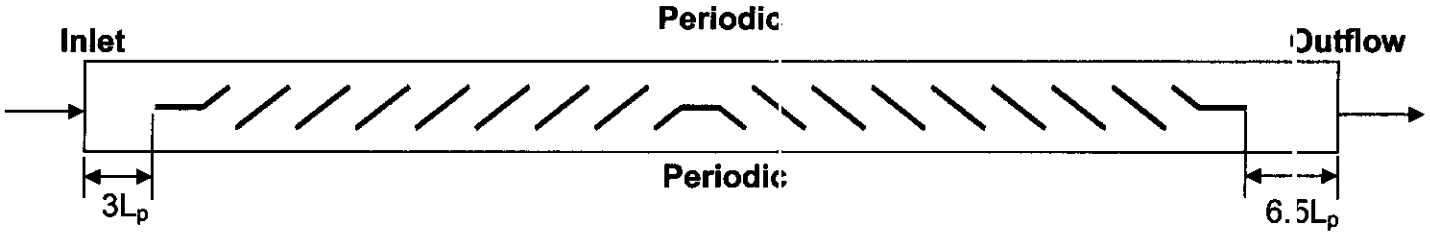

Figure 2 Boundary conditions used for the computational simulations performed during this study.

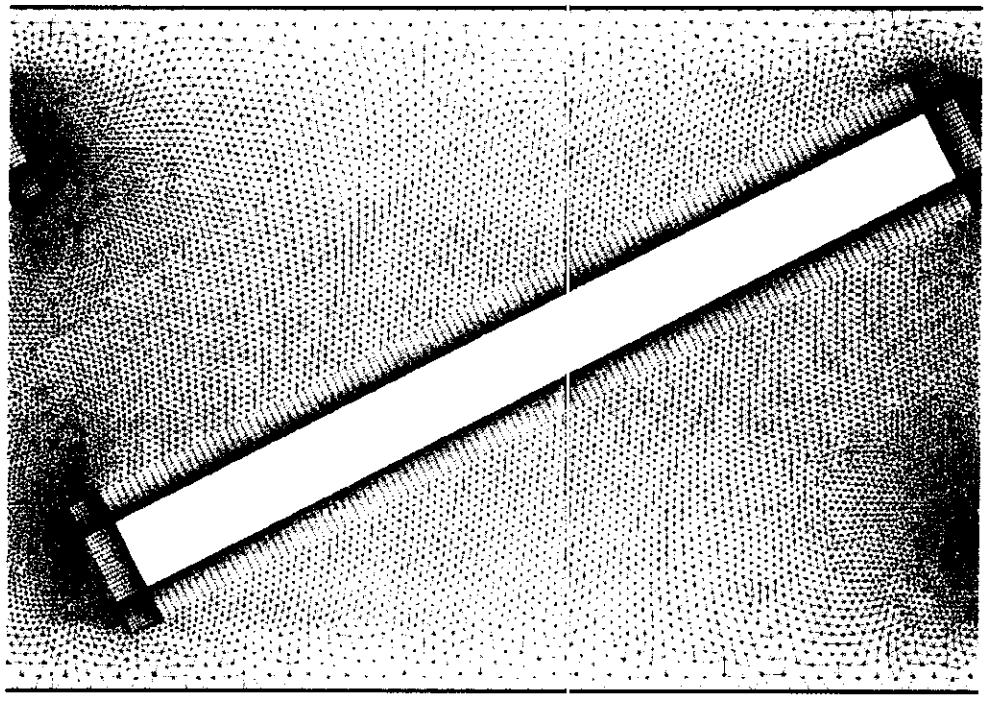

Figure 3 A portion of the CFD grid showing a detailed section of the quadrilateral (boundary layer) grid used around each of the louvers.

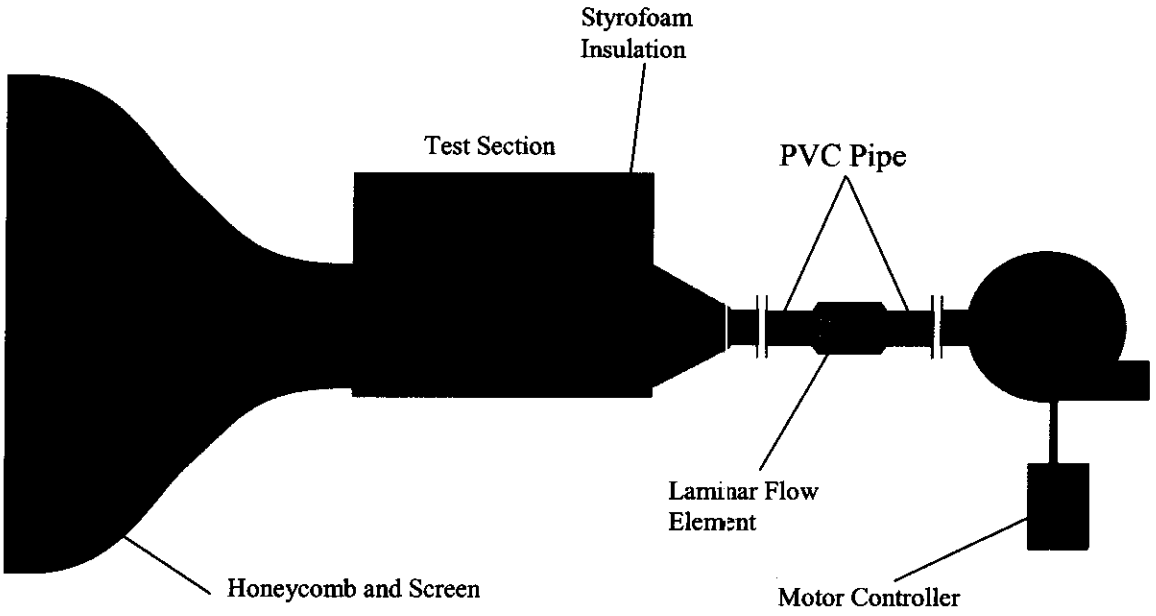

Figure 4 The test facility used for the heat transfer measurements along the scaled-up louvers.

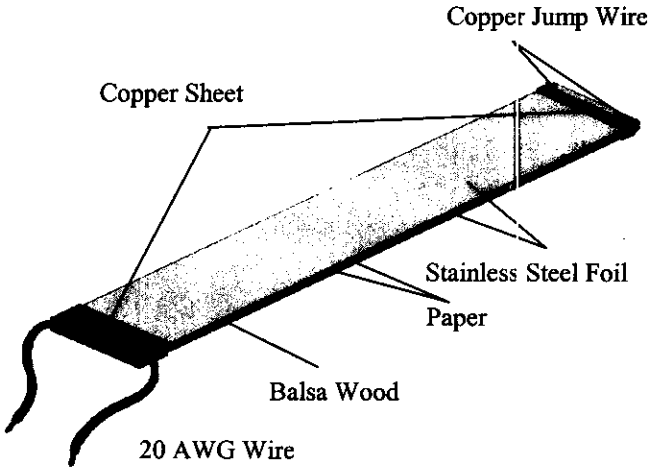

Figure 5 The heated louver design used during the experiments.

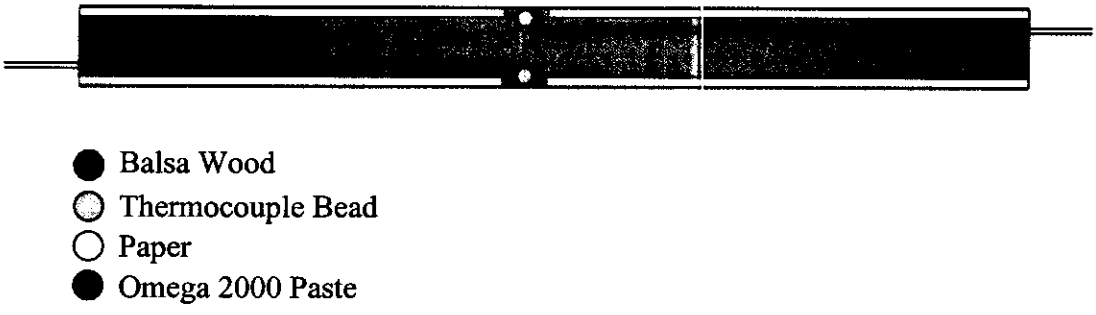

Figure 6 Cross-sectional view of an instrumented louver.

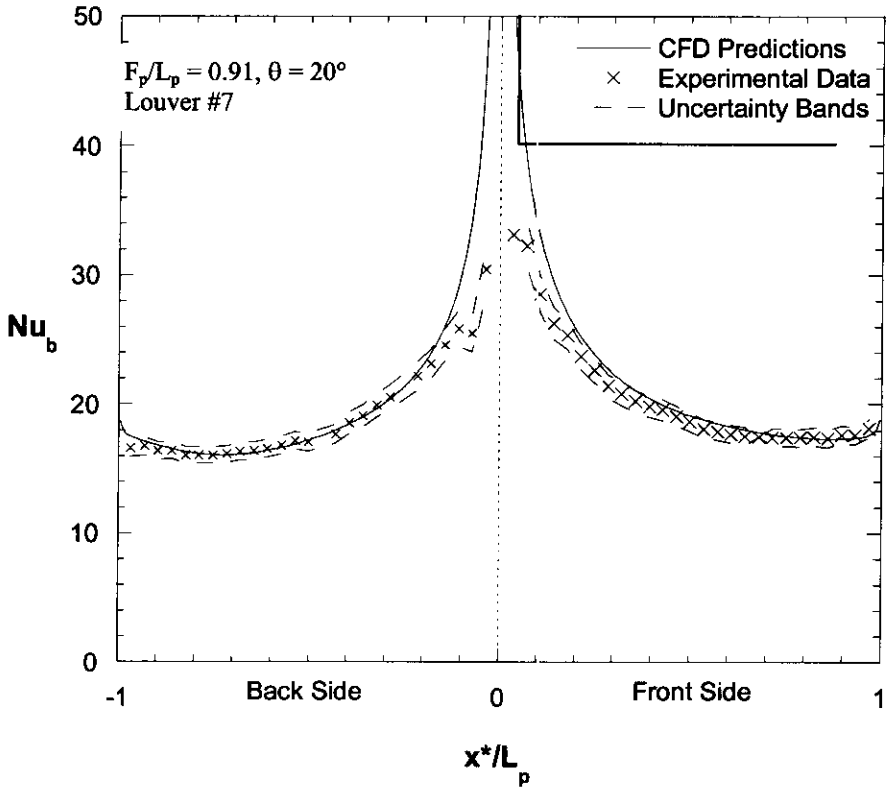

Figure 8 Comparison of the experimental data and the CFD data for the Nusselt number at louver 7 for the $F_p/L_p = 0.91$, $\theta = 20°$ model at $Re_{Lp} = 1016$.

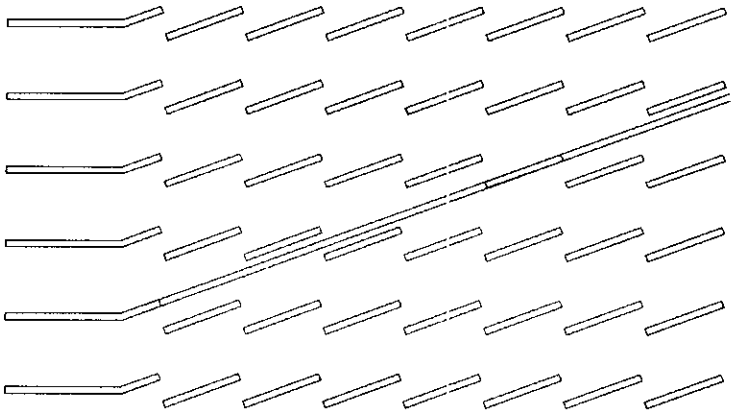

Figure 9 Entrance louver's alignment shown with the louvers impacted by thermal wakes for the $F_p/L_p = 0.91$, $\theta = 20°$ model at $Re_{Lp} = 230$.

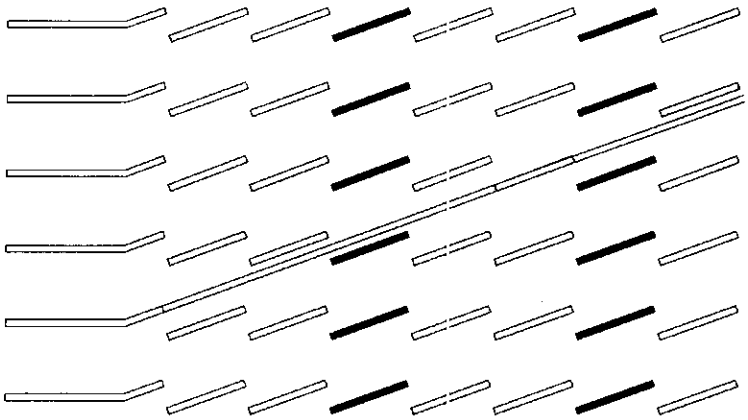

Figure 10 Entrance louver's alignment shown with the louvers impacted by thermal wakes for the $F_p/L_p = 0.91$, $\theta = 20°$ model at $Re_{Lp} = 1016$.

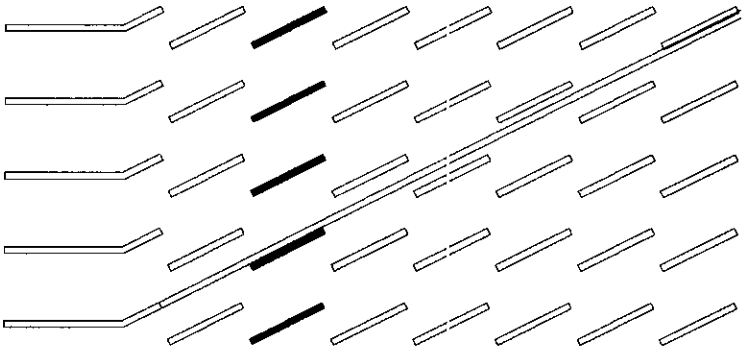

Figure 11 Entrance louver's alignment shown with the louvers impacted by thermal wakes for the $F_p/L_p = 0.91$, $\theta = 27°$ model at $Re_{Lp} = 230$.

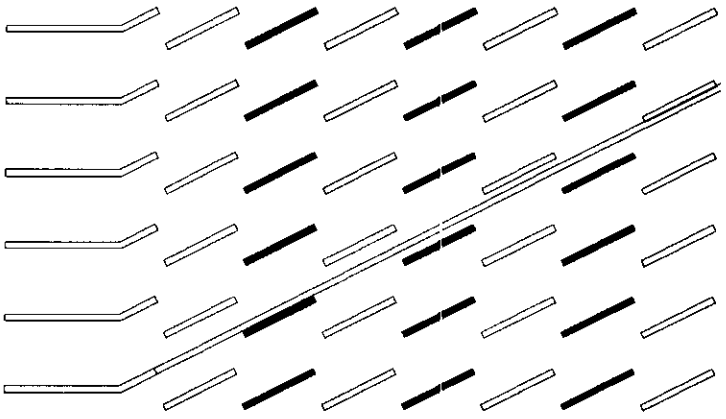

Figure 12 Entrance louver's alignment shown with the louvers impacted by thermal wakes for the $F_p/L_p = 0.91$, $\theta = 27°$ model at $Re_{Lp} = 1016$.

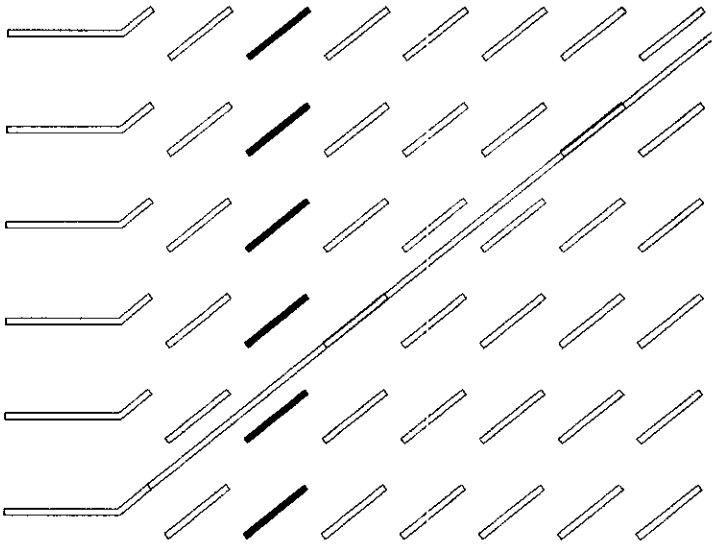

Figure 13 Entrance louver's alignment shown with the louvers impacted by thermal wakes for the $F_p/L_p = 1.22$, $\theta = 39°$ model at $Re_{Lp} = 1016$.

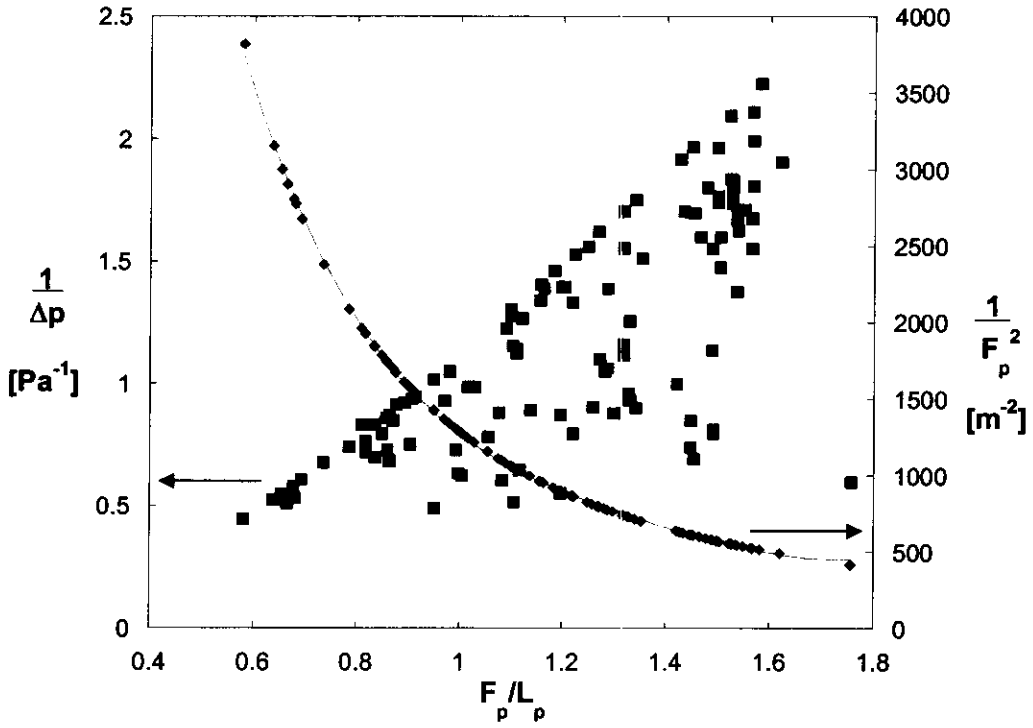

Figure 14 CFD optimization results with the optimization function shown as two parts.

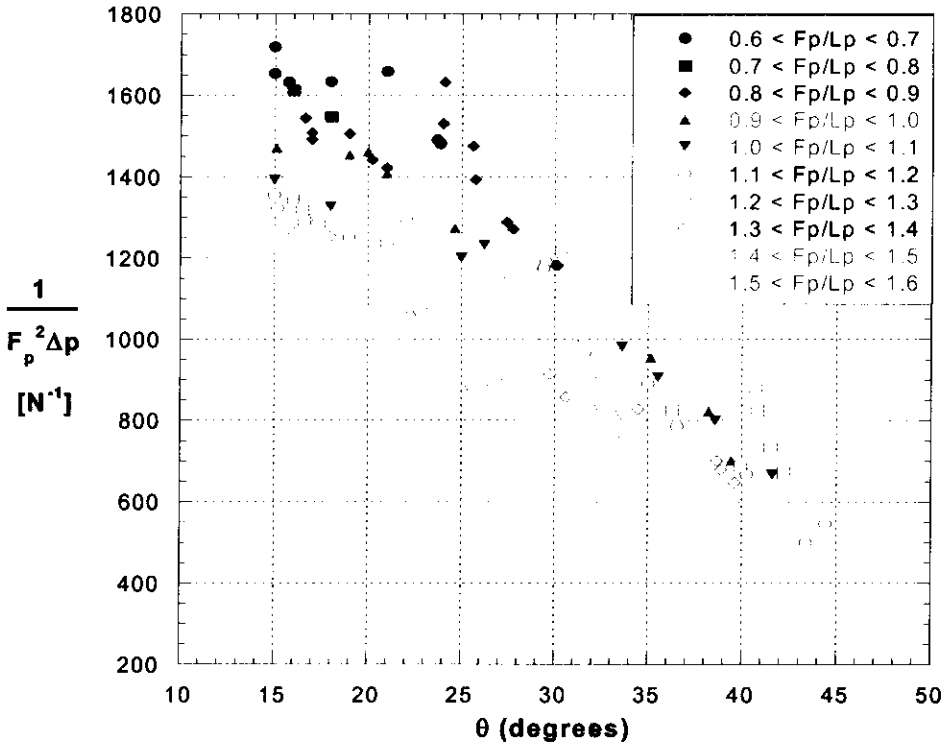

Figure 15 CFD optimization results showing the louver angle effect on the optimization function.

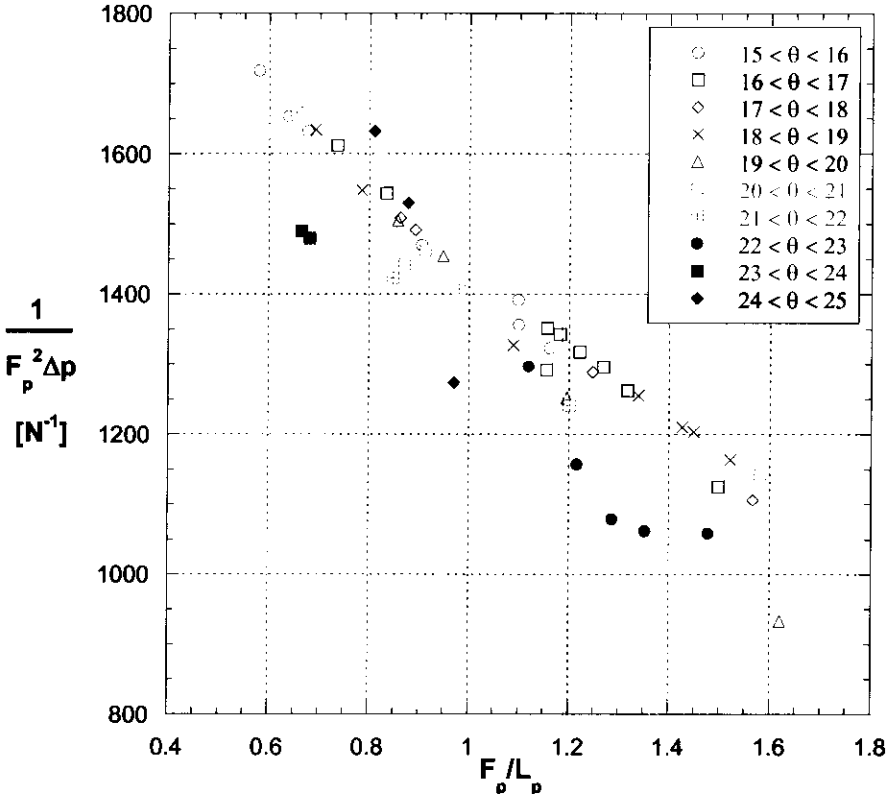

Figure 16 CFD optimization results showing the effect of F_p/L_p on the optimization function for $15°<\theta<25°$.

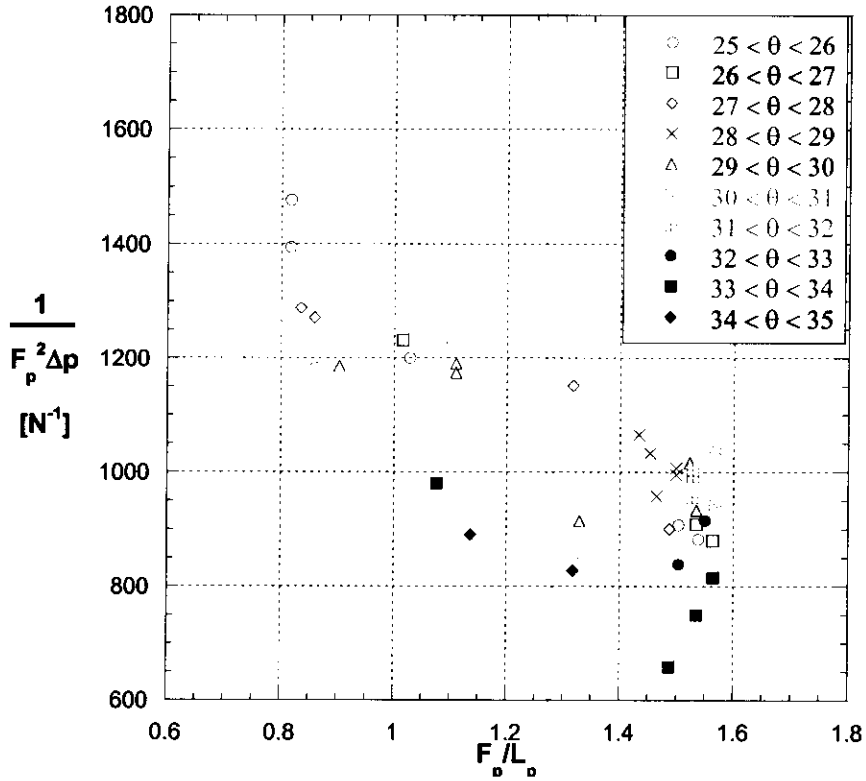

Figure 17 CFD optimization results showing the effect of F_p/L_p on the optimization function for $25°<\theta<35°$.

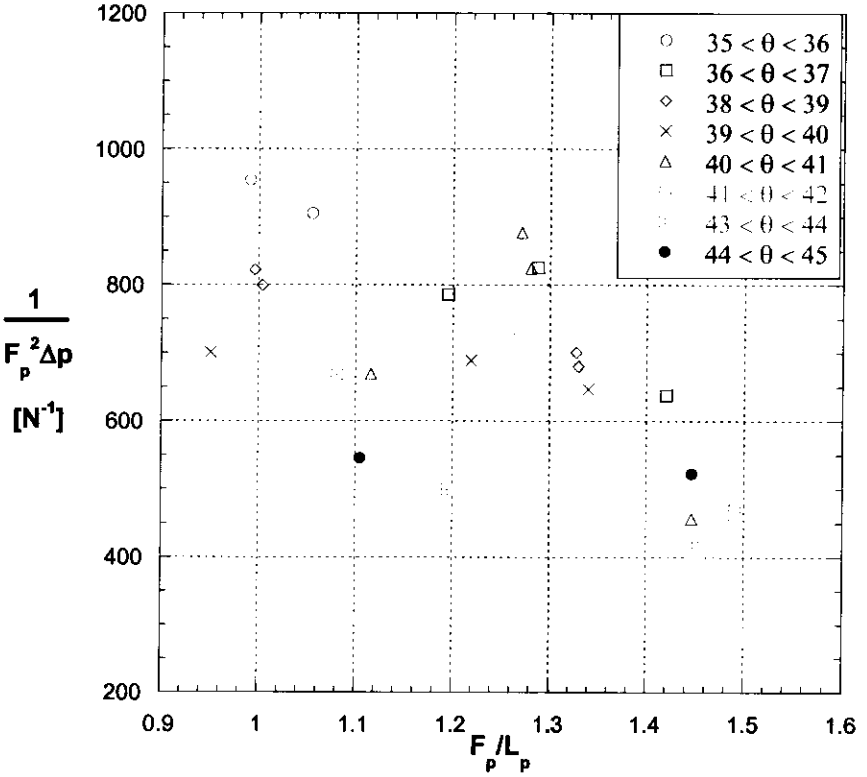

Figure 18 CFD optimization results showing the effect of F_p/L_p on the optimization function for $35°<\theta<45°$.